

# ForensicZip: More Tokens are Better but Not Necessary in Forensic Vision-Language Models

Yingxin Lai<sup>1</sup>, Zitong Yu<sup>1\*</sup>, Jun Wang<sup>1\*</sup>, Linlin Shen<sup>2</sup>, Yong Xu<sup>3</sup>, and Xiaochun Cao<sup>4</sup>

<sup>1</sup> Great Bay University

<sup>2</sup> Shenzhen University

<sup>3</sup> Harbin Institute of Technology

<sup>4</sup> School of Cyber Science and Technology, Sun Yat-sen University  
{yingxinlai20}@gmail.com

**Abstract.** Multimodal Large Language Models (MLLMs) enable interpretable multimedia forensics by generating textual rationales for forgery detection. However, processing dense visual sequences incurs high computational costs, particularly for high-resolution images and videos. Visual token pruning is a practical acceleration strategy, yet existing methods are largely semantic-driven, retaining salient objects while discarding background regions where manipulation traces such as high-frequency anomalies and temporal jitters often reside. To address this issue, we introduce ForensicZip, a training-free framework that reformulates token compression from a forgery-driven perspective. ForensicZip models temporal token evolution as a Birth-Death Optimal Transport problem with a slack dummy node, quantifying physical discontinuities indicating transient generative artifacts. The forensic scoring further integrates transport-based novelty with high-frequency priors to separate forensic evidence from semantic content under large-ratio compression. Experiments on deepfake and AIGC benchmarks show that at 10% token retention, ForensicZip achieves  $2.97\times$  speedup and over 90% FLOPs reduction while maintaining state-of-the-art detection performance. Code is publicly available at <https://github.com/laiyingxin2/ForensicZip>.

**Keywords:** Multimedia Forensics · Visual Token Pruning · Multimodal Large Language Models

## 1 Introduction

Recent advances in Multimodal Large Language Models (MLLMs) [2, 8, 23–25, 33, 38] have led to remarkable progress in building generalist systems for diverse visual understanding and reasoning tasks. In multimedia forensics, MLLMs are increasingly adopted as an explainable pathway for forgery detection. With large-scale visual instruction tuning, forensic MLLMs [15, 19, 32, 40, 50] can not only predict authenticity but also produce fine-grained textual rationales, such as pointing out abnormal clues, blending boundaries, or inconsistent reflections [6, 36]. However, practical deployment remains challenging. To capture subtle manipulation traces, these models must process high-resolution images or long video streams. This mechanism generates a massive number of visual tokens, making the prefilling stage a computational bottleneck due to the heavy computational cost of self-attention.

A growing line of work shows that visual tokens in Vision-Language Models (VLMs) and MLLMs are highly redundant, motivating training-free token pruning and merging as a practical inference acceleration strategy [16, 42]. Representative methods perform early-layer pruning [4, 37], attention- or sparsity-guided token selection [27, 46], or adaptive token reduction [28, 31]. Most of these approaches rank tokens by semantic salience (e.g., cross-modal attention, vision-language similarity, or macro-diversity [1, 22]) and achieve substantial compute savings with minor performance drops on standard benchmarks such as captioning [12, 44] and VQA [43, 49].

Despite this progress, semantic-driven token reduction is often misaligned with the forgery-driven requirements of forensic detection. Key manipulation cues (such as high-frequency noise patterns, subtle blending seams, or transient temporal jitters) tend to be weakly correlated with object-level semantics. They are often distributed in visually flat regions that semantic criteria treat as redundant [37, 42, 48]. Meanwhile, recent analyses report that text-guided attention can exhibit cross-modal misalignment inside MLLM layers, making semantic scores unreliable under compression [39, 45]. Consequently, current methods tend to over-retain macro-semantic objects while discarding low-saliency regions that still contain forensic evidence, leading to significant performance degradation at high pruning ratios, as illustrated in Fig. 2(a). These observations motivate three questions: (1) Why do existing pruning methods suffer task-dependent degradation on forgery detection? (2) How do generative artifacts manifest dynamically in the visual token space, especially over time? (3) How can we aggressively compress visual tokens while preserving subtle, non-salient forensic evidence?

In this work, we observe that many modern generation pipelines, despite strong per-frame realism, often violate physical continuity across frames. In the visual token space, such violations manifest as transient birth and death events of local

\* Corresponding authors.

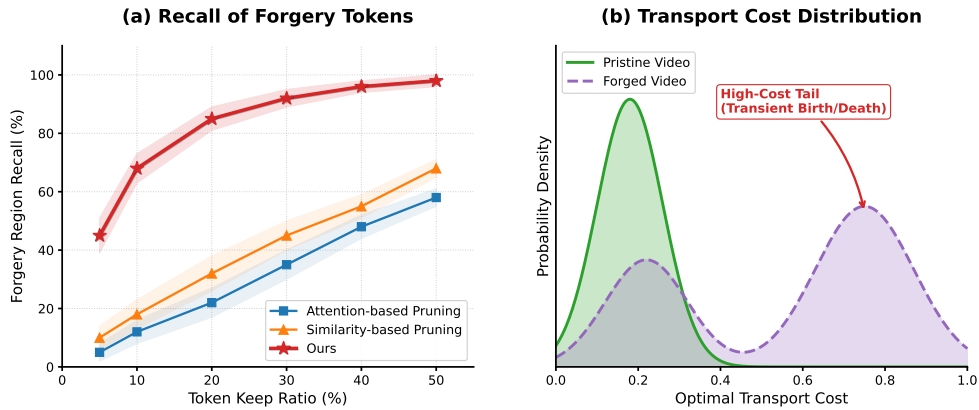


**Fig. 1: Quantitative analysis of forensic-semantic misalignment.** (a) Recall of retained tokens against ground-truth forgery regions under varying compression ratios. Semantic-driven criteria show high sensitivity to compression ratios, while our transport-based novelty score maintains stable coverage of localized anomalies. Shaded regions denote  $\pm 1$  standard deviation across evaluation samples. (b) Distribution of temporal Optimal Transport (OT) costs. The distinct high-cost tail in forged videos indicates physical discontinuities (birth-death events), supporting the use of our augmented OT formulation.

textures and structures (Fig. 2b). Building on this insight, we propose ForensicZip, a training-free token compression framework that shifts the paradigm from semantic-driven pruning to forgery-driven sparsification. ForensicZip consists of two core components: First, Transport Novelty Estimation (TNE) formulates temporal token evolution as an augmented entropic Optimal Transport problem. By introducing a dummy node, it explicitly translates physical incoherence into quantifiable birth and death costs. Second, Forensic Scoring integrates these transport costs with frequency-domain priors and applies distance-penalized stabilization to separate forensic signals from semantic content. Finally, based on these stabilized scores, we perform a physical Top- $K$  selection, yielding genuine sequence-length reduction and end-to-end acceleration. Our contributions are summarized as follows:

- **Task-specific Analysis:** We identify a structural mismatch between semantic-driven token pruning and the forgery-driven nature of forgery detection, demonstrating that preserving global anchors and transient artifacts is crucial under aggressive token budgets.
- **ForensicZip Framework:** We propose a training-free token sparsification framework that leverages augmented Birth-Death Optimal Transport for forensic novelty estimation, together with a frequency-aware scoring strategy for robust evidence preservation.
- **Performance Validation:** ForensicZip seamlessly integrates into existing forensic MLLMs via physical pruning. Extensive experiments across deepfake and AIGC benchmarks demonstrate that at an aggressive 10% token retention, our method achieves  $2.97\times$  speedup and reduces FLOPs by over 90% while maintaining state-of-the-art detection performance.

## 2 Related Work

*Synthetic Image Detection via MLLMs.* Deepfake and synthetic image detection have shifted from binary classification [7, 17, 29, 34, 35] to interpretable forensics using Multimodal Large Language Models (MLLMs). Recent methods bridge visual anomalies with natural-language rationales via common-sense [47] or pattern-aware reasoning [32], and language-guided localization [14]. To enhance transparency, frameworks like FakeShield [40], X2-DFD [6], and Spot the Fake [36] generate fine-grained explanations paired with spatial masks. This paradigm extends to diverse domains, including face forensics [15], diffusion videos [30], and social media (e.g., SIDA [19]), culminating in comprehensive forensic assistants like AIGI-Holmes [50] and LEGION [20]. Despite these advances, these methods typically assume a sufficient computational budget to process dense visual tokens, neglecting the severe prefill latency bottleneck in high-resolution or long-video scenarios.

*Visual Token Compression for Efficient MLLM Inference.* Visual token reduction mitigates redundancy and accelerates MLLM inference. One prominent line of research relies on semantic importance to rank tokens via early-layer [4, 5] or text-to-vision attention [46]. To improve information density and coverage, recent approaches employ clustering [31, 48] or diversity-based selection [1, 22] to prevent token over-concentration. For video and high-resolution scenarios, frameworks explicitly exploit spatio-temporal dynamics [37] or offer training-free plug-and-play pipelines [16, 26] to reduce redundancy. Despite this progress, existing methods remain fundamentally semantic-driven, prioritizing macro-level visual understanding. In contrast, forensic cues are intrinsically anti-semantic localized artifacts like resampling patterns or temporal jitters

frequently reside in regions deemed redundant by conventional metrics. Furthermore, recent analyses [13, 45] reveal that semantic pruning under cross-modal misalignment can destroy the global spatial reference required for precise forgery localization. These limitations motivate our ForensicZip framework, which formulates token evolution as an optimal transport problem to preserve non-semantic forensic evidence while achieving physical sequence-length reduction.

### 3 ForensicZip

We first review the forensic VLM pipeline and analyse why visual sequence length is the primary efficiency bottleneck (Sec. 3.1). We then present two empirical observations that reveal a structural mismatch between semantic-driven token pruning and forgery detection (Sec. 3.2). Finally, Sec. 3.3 introduces our training-free scoring and selection procedure, which retains a small token subset per frame based on physical inconsistency rather than conceptual saliency.

#### 3.1 Preliminary

*Forensic VLM pipeline.* A typical forensic VLM consists of a vision encoder, a multimodal projector  $g : \mathbb{R}^{D_v} \rightarrow \mathbb{R}^{D_p}$ , and a language model, where  $D_v$  is the vision-encoder hidden dimension and  $D_p$  is the language embedding dimension. Given a video with  $T$  frames  $\{\mathbf{I}_t\}_{t=1}^T$ , the vision encoder produces, for each frame  $t$ , one global token and  $N$  patch tokens  $\mathbf{V}_t = \{\mathbf{v}_{t,1}, \dots, \mathbf{v}_{t,N}\} \in \mathbb{R}^{N \times D_v}$ , where  $\mathbf{v}_{t,i} \in \mathbb{R}^{D_v}$  is the  $i$ -th patch token.

*Sequence-length complexity.* For a transformer with  $L_{\text{layer}}$  layers, sequence length  $n$ , hidden size  $d$ , and FFN intermediate size  $m$ , the FLOPs are approximated by

$$\text{FLOPs} = L_{\text{layer}}(4nd^2 + 2n^2d + 2ndm). \quad (1)$$

The quadratic self-attention term  $2n^2d$  makes cost sensitive to  $n$ . In multimodal prompting the total length decomposes as

$$n = n_{\text{sys}} + n_{\text{vis}} + n_{\text{txt}}, \quad n_{\text{vis}} = T(N + 1), \quad (2)$$

where  $n_{\text{sys}}$ ,  $n_{\text{txt}}$ , and  $n_{\text{vis}}$  denote system-prompt, user-text, and visual-token lengths, respectively. Because  $n_{\text{vis}}$  dominates in high-resolution and video settings, reducing visual tokens directly lowers prefill cost and memory footprint [1, 3, 37, 42].

#### 3.2 The Forensic-Semantic Discrepancy

Before presenting our framework, we investigate how common token reduction paradigms behave in the forensic domain. Through systematic analysis on the FakeVLM benchmark, we identify two misalignments that together motivate a transport-based scoring mechanism with explicit slack.

*Obs. 1: Inverse correlation between semantic saliency and forensic evidence.* Existing pruning strategies assume that semantically salient regions carry the most task-critical information. As shown in Fig. 2(a), however, we observe a systematic inverse correlation between cross-modal attention magnitude and spatial overlap with ground-truth forgery masks. MLLM attention heads converge on high-level object centres, whereas manipulation traces such as blending inconsistencies, resampling grids, and compression artefacts reside predominantly in low-saliency backgrounds and object edges. Purely semantic reduction therefore acts as a low-pass filter on forensic information, preserving convincing content while removing the subtle evidence required for detection.

*Obs. 2: Temporal discontinuity as Birth–Death events.* We further examine token dynamics in the projected feature space across adjacent frames. In pristine video, tokens evolve smoothly: under uniform marginals the optimal transport plan between consecutive frames concentrates mass along the cost-matrix diagonal, reflecting continuous spatial correspondence. Generative models violate this continuity: certain features appear without a plausible source (Birth) or vanish without a matching target (Death). As shown in Fig. 2(b), conventional nearest-neighbour or balanced matching forces these outliers into spurious correspondences. Because the anomalous mass is then distributed across many low-cost entries rather than concentrated in a single high-cost event, the forgery signal is diluted below a practical detection threshold. This dilution effect motivates an unbalanced transport formulation that can explicitly route unmatchable mass through a dedicated slack node.

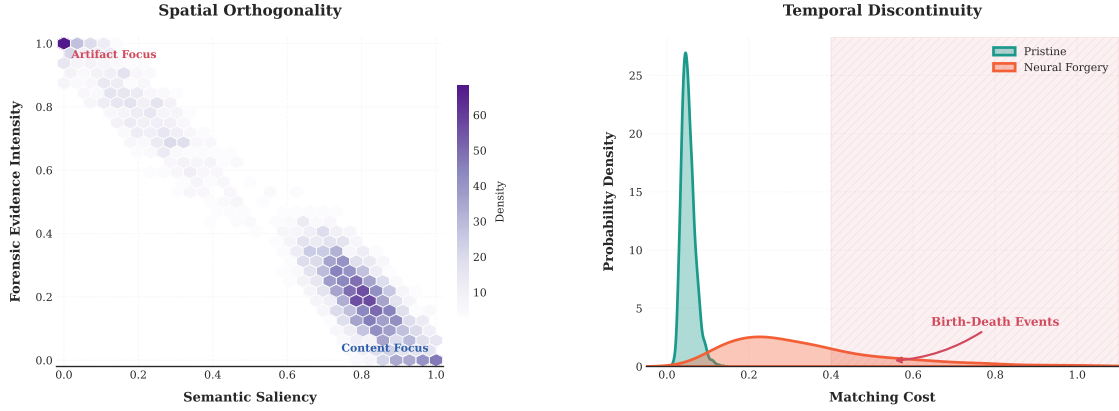


**Fig. 2: Empirical motivation for ForensicZip.** (a) **Inverse Correlation:** Density plot of semantic saliency (cross-modal attention) vs. forensic evidence (IoU with forgery masks) on FakeClue/LOKI. (b) **Temporal Discontinuity:** KDE of inter-frame matching costs.

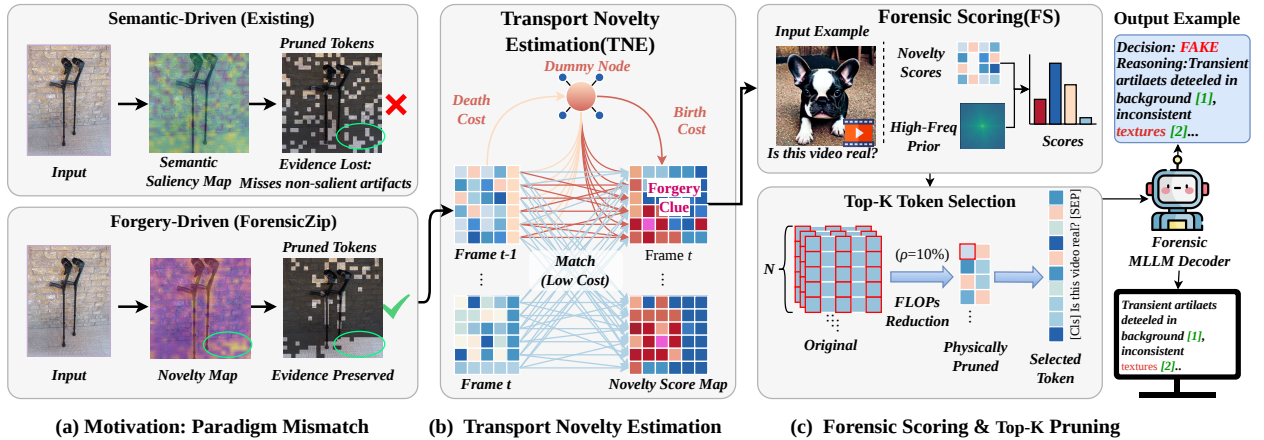


**Fig. 3: Overall framework of ForensicZip.** ForensicZip measures transport novelty across adjacent video frames and selectively preserves vision tokens with high physical inconsistency (i.e., transient artifacts), thereby achieving plug-and-play forensic MLLM inference acceleration.

### 3.3 Methodology

Both observations point to a single principle: forensic evidence resides where physical conservation laws are violated, not where semantic content is concentrated. Generation pipelines leave frequency-domain fingerprints in the spatial domain (Obs. 1) and break feature-level mass conservation in the temporal domain (Obs. 2). We realise this principle through two complementary stages (Fig. 3). *Transport Novelty Estimation* (TNE) detects temporal violations by modelling inter-frame correspondence as an augmented optimal transport problem with a slack node, so that unmatched mass surfaces as concentrated Birth–Death costs. *Forensic Scoring* (FS) detects spatial violations by modulating the temporal scores with a high-frequency prior. Their product implements a soft AND gate: only tokens anomalous in both domains receive high scores.

**Transport Novelty Estimation (TNE)** Forgery detection in the temporal domain reduces to conservation violation detection: natural video preserves feature-level mass across frames, whereas generative artefacts create or destroy local textures abruptly. A naïve cosine-similarity approach treats each token independently, so anomalous residuals are absorbed by the single best match. Optimal transport improves on this by finding a global assignment under marginal constraints, but standard balanced OT enforces strict mass conservation, forcing every target token onto a real source and smearing the anomaly across many small residuals. Adding a dummy node closes this gap: tokens that genuinely lack a predecessor can route their mass through the dummy at a fixed penalty, surfacing as concentrated high-cost events.

*Birth–Death entropic optimal transport.* Each patch token  $\mathbf{v}_{t,i} \in \mathbb{R}^{D_v}$  ( $i = 1, \dots, N$ ) in frame  $t$  is projected and  $\ell_2$ -normalised:

$$\hat{\mathbf{z}}_{t,i} = \frac{g(\mathbf{v}_{t,i})}{\|g(\mathbf{v}_{t,i})\|_2 + \epsilon_{\text{norm}}}, \quad \hat{\mathbf{z}}_{t,i} \in \mathbb{R}^{D_p}, \quad (3)$$

where  $\epsilon_{\text{norm}}$  is a small constant for numerical stability. Normalisation maps all embeddings onto the unit hypersphere, naturally yielding cosine distance as the ground cost.

For consecutive frames  $(t-1, t)$  with  $T \geq 2$ , we build a pairwise cost matrix  $\mathbf{C}^{(t)} \in \mathbb{R}^{N \times N}$  whose entry  $C_{ij}^{(t)} = 1 - \hat{\mathbf{z}}_{t-1,i}^\top \hat{\mathbf{z}}_{t,j}$  measures the cosine distance between the  $i$ -th source token in frame  $t-1$  and the  $j$ -th target token in frame  $t$ . To flag tokens that appear without a source (*Birth*) or vanish without a target (*Death*), we extend this matrix with a dummy row and column:

$$\bar{\mathbf{C}}^{(t)} = \begin{bmatrix} \mathbf{C}^{(t)} & c_{\text{death}} \mathbf{1}_N \\ c_{\text{birth}} \mathbf{1}_N^\top & 0 \end{bmatrix} \in \mathbb{R}^{(N+1) \times (N+1)}, \quad (4)$$

where  $\mathbf{1}_N \in \mathbb{R}^N$  is the all-ones vector. The scalar penalties  $c_{\text{birth}} \geq 0$  and  $c_{\text{death}} \geq 0$  set the cost of routing mass through the dummy node: whenever the cheapest real assignment of a target token exceeds  $c_{\text{birth}}$ , the solver preferentially explains it as a newly appeared artefact. Instead of forcing a spurious pairing that dilutes the anomaly, the dummy node absorbs the unmatched mass and concentrates the cost into a single interpretable entry.

We impose marginals  $\mathbf{a} = [\frac{1}{N}, \dots, \frac{1}{N}, 1]^\top \in \mathbb{R}^{N+1}$ , where the first  $N$  entries assign uniform mass to real tokens and the last entry provides unit slack to absorb all unmatched mass if necessary. The entropic transport plan  $\bar{\mathbf{P}}^{(t)} \in \mathbb{R}^{(N+1) \times (N+1)}$  is obtained via  $I_{\text{sk}}$  Sinkhorn iterations (set to 20 in all experiments):

$$\bar{\mathbf{P}}^{(t)} = \arg \min_{\mathbf{P} \geq 0, \mathbf{P} \mathbf{1}_{N+1} = \mathbf{a}, \mathbf{P}^\top \mathbf{1}_{N+1} = \mathbf{a}} \langle \mathbf{P}, \bar{\mathbf{C}}^{(t)} \rangle_F + \varepsilon_{\text{ot}} \sum_{i=1}^{N+1} \sum_{j=1}^{N+1} P_{ij} (\log P_{ij} - 1), \quad (5)$$

where  $\langle \cdot, \cdot \rangle_F$  denotes the Frobenius inner product,  $\varepsilon_{\text{ot}} > 0$  is the entropic regularisation strength, and  $\mathbf{1}_{N+1} \in \mathbb{R}^{N+1}$  is the  $(N+1)$ -dimensional all-ones vector used in the marginal constraints.

*Per-token score extraction.* From the solved plan we extract two scores for each target token  $j$  ( $j = 1, \dots, N$ ) in frame  $t$ , spanning the full range of temporal anomaly from gradual drift to abrupt appearance. The *transport cost* aggregates the weighted matching cost from all  $N$  real source tokens in frame  $t-1$ , excluding the dummy row:

$$e_j^{(t)} = \sum_{i=1}^N \bar{P}_{ij}^{(t)} C_{ij}^{(t)}. \quad (6)$$

A high  $e_j^{(t)}$  indicates that token  $j$  deviates from every predecessor yet was still partially matched, capturing distributed anomalies. The *Birth evidence*

$$b_j^{(t)} = \bar{P}_{N+1,j}^{(t)} \quad (7)$$

records the mass routed from the dummy source, directly quantifying the absence of a plausible origin in frame  $t-1$  and capturing abrupt appearance that admits no real correspondence.

For single-image inputs ( $T = 1$ ), the module falls back to a spatial mode: we compute the frame-level mean embedding  $\boldsymbol{\mu} = \frac{1}{N} \sum_{j=1}^N \hat{\mathbf{z}}_{1,j}$  and define per-token novelty as  $s_j^{(1)} = \|\hat{\mathbf{z}}_{1,j} - \boldsymbol{\mu}\|_2$ .

Transport cost measures feature-level displacement but is agnostic to its cause: legitimate large-scale motion such as camera panning produces elevated cost indistinguishable from a generative artefact on the basis of temporal signal alone. Resolving this ambiguity requires a signal from a different physical domain.

**Forensic Scoring and Selection (FS)** Generative artefacts and natural motion differ not in temporal displacement magnitude but in spatial frequency signature. Natural motion displaces existing textures without altering their local spectral statistics, whereas generation pipelines introduce characteristic fingerprints: aliasing from resampling, spectral gaps from upsampling networks, and gradient discontinuities at blending boundaries. This frequency-domain signal also addresses the inverse correlation identified in Obs. 1: forensic traces in semantically flat regions still carry strong high-frequency responses and are therefore preserved.

*High-frequency prior integration.* We apply a fixed  $3 \times 3$  Laplacian operator  $\mathcal{L}(\cdot)$  to the input frame  $\mathbf{I}_t$  and average-pool the response to the  $N$ -element patch grid, yielding a spatial proxy  $\mathbf{U}^{(t)} \in [0, 1]^N$  where  $U_j^{(t)}$  is the normalised response at the  $j$ -th patch position. The forensic score for token  $j$  in frame  $t$  is the product of a temporal anomaly term and a spatial modulation term:

$$s_j^{(t)} = \underbrace{(e_j^{(t)} + \lambda_{\text{birth}} b_j^{(t)})}_{\text{temporal anomaly}} \cdot \underbrace{(1 + \eta_{\text{forensic}} U_j^{(t)})}_{\text{spatial modulation}}, \quad (8)$$

**Table 1: Quantitative Performance of ForensicZip on FakeVLM and FakeShield Backbones.** “Vanilla” denotes the full-token upper bound. **Avg. Lat. (ms)** is end-to-end per-sample inference latency, **GPU Mem. (GB)** is peak GPU memory, and **Speedup** is w.r.t. Vanilla; efficiency metrics are averaged over all datasets in this table. (*Red text indicates performance collapse.*)

Method	Backbone: FakeVLM				Backbone: FakeShield				Avg. FLOPs(T)	Avg. Lat.(ms)	GPU Mem.(GB)	Speedup
	FakeClue	LOKI	DD-VQA	DMimage	PhotoShop	DeepFake	AIGC	DFFD				
<i>Upper Bound (100% Tokens)</i>												
Vanilla	98.60	84.30	93.20	94.00	94.43	98.00	93.00	98.00	3.102	4520.2	26.7	1.00×
<i>Retain 50% Tokens</i> (↓ 50% visual tokens)												
FastV (ECCV’24)	95.23	78.15	89.52	88.24	90.15	93.42	88.54	93.22	2.150	3228.6	26.6	1.40×
SparseVLM (ICML’25)	96.14	79.53	90.45	89.66	91.24	94.15	89.23	94.44	2.155	3180.4	26.5	1.42×
LLaVA-Scissor (NeurIPS’25)	97.22	81.84	91.81	91.13	92.83	95.84	91.42	95.85	2.140	3110.5	26.7	1.45×
VisionTrim (ICLR’26)	97.87	82.25	92.92	92.34	93.54	96.92	92.15	96.52	2.135	3090.2	26.4	1.46×
<b>ForensicZip (Ours)</b>	<b>98.50</b>	<b>84.35</b>	<b>93.25</b>	<b>94.05</b>	<b>94.48</b>	<b>98.05</b>	<b>93.05</b>	<b>98.04</b>	<b>1.852</b>	<b>2756.4</b>	<b>22.4</b>	<b>1.64×</b>
<i>Retain 25% Tokens</i> (↓ 75% visual tokens)												
FastV (ECCV’24)	82.34	65.55	76.42	75.13	78.25	81.52	75.43	80.84	1.420	2510.5	26.5	1.80×
SparseVLM (ICML’25)	85.63	68.22	79.65	78.54	81.42	83.15	78.56	83.22	1.415	2480.8	26.4	1.82×
LLaVA-Scissor (NeurIPS’25)	91.45	75.53	86.24	85.42	86.54	90.45	85.13	90.92	1.390	2420.2	26.6	1.86×
VisionTrim (ICLR’26)	94.83	79.15	89.56	89.24	90.25	94.14	89.55	94.83	1.385	2390.6	26.3	1.89×
<b>ForensicZip (Ours)</b>	<b>98.46</b>	<b>83.93</b>	<b>93.12</b>	<b>93.88</b>	<b>94.32</b>	<b>97.88</b>	<b>92.85</b>	<b>97.82</b>	<b>0.985</b>	<b>2050.5</b>	<b>19.8</b>	<b>2.20×</b>
<i>Retain 10% Tokens</i> (↓ 90% visual tokens)												
FastV (ECCV’24)	60.54	45.13	56.42	55.25	55.93	58.54	53.22	57.83	0.850	1950.2	26.4	2.31×
SparseVLM (ICML’25)	65.82	48.45	60.14	59.53	60.25	63.83	58.14	61.52	0.845	1920.5	26.3	2.35×
LLaVA-Scissor (NeurIPS’25)	78.25	62.53	72.56	71.24	72.54	76.12	71.43	75.85	0.820	1880.8	26.5	2.40×
VisionTrim (ICLR’26)	84.53	70.84	80.25	78.56	79.14	82.55	76.82	82.24	0.815	1850.4	26.1	2.44×
<b>ForensicZip (Ours)</b>	<b>97.74</b>	<b>82.15</b>	<b>90.58</b>	<b>91.23</b>	<b>92.15</b>	<b>95.88</b>	<b>90.85</b>	<b>95.62</b>	<b>0.452</b>	<b>1520.3</b>	<b>18.5</b>	<b>2.97×</b>

where  $\lambda_{\text{birth}} \geq 0$  balances Birth evidence against transport cost, and  $\eta_{\text{forensic}} \geq 0$  controls the amplification from high-frequency features. The multiplicative form implements a soft AND gate: a token must carry both temporal novelty and spatial edge activity to score highly. An additive alternative would let a uniformly displaced background patch (high transport cost, zero frequency response) dominate the ranking during camera panning, while a static object boundary (strong edges, zero temporal novelty) would collapse the score into a generic edge detector. The product suppresses both cases because zeroing either factor eliminates the score.

*Token selection.* Given a retention ratio  $\rho \in (0, 1]$ , we select the top  $K = \lfloor \rho N \rfloor$  tokens from  $\{s_j^{(t)}\}_{j=1}^N$  for each frame  $t$ , where  $K$  denotes the retained patch count per frame. The global token is always kept. The compressed sequence of length  $T(K+1)$  replaces the original  $T(N+1)$  tokens and is passed directly to the language model.

**Computational Complexity** Each transformer layer incurs  $\mathcal{O}(n^2 D_m + n D_m D_{\text{ff}})$  cost, where  $n$  is the token count,  $D_m$  is the language-model hidden dimension, and  $D_{\text{ff}}$  is the FFN intermediate size. Reducing the per-frame visual sequence from  $N+1$  to  $K+1$  tokens across all  $L_{\text{layer}}$  layers eliminates the dominant quadratic term by a factor of  $1 - (K+1)^2/(N+1)^2$  per layer. The only overhead is the entropic OT solver on an  $(N+1) \times (N+1)$  cost matrix:

$$\text{Cost}_{\text{OT}} = \mathcal{O}((T-1) I_{\text{sk}} (N+1)^2), \quad (9)$$

where  $I_{\text{sk}}$  is the number of Sinkhorn iterations and  $T-1$  is the number of consecutive frame pairs. Because this cost is incurred once before the LLM forward pass and scales linearly with frame count, it is negligible relative to the multi-layer transformer savings. **A detailed theoretical analysis is provided in the supplementary material.**

## 4 Experiments

**Benchmarks.** To evaluate ForensicZip across diverse forgery types, we utilize three dataset categories: (1) **Universal & AIGC Detection:** FakeVLM (FakeClue, LOKI [41]), DMimage [9], FakeShield-AIGC [40], and SIDA [18] for synthetic artifacts and social media imagery; (2) **DeepFake Forensics:** DD-VQA [47] for artifact explanation, alongside FakeShield-DeepFake and DFFD [10] for facial manipulation; and (3) **Traditional Manipulation:** FakeShield-PhotoShop (aggregating CASIA [11], etc.) for splicing and copy-move forgeries, and the commonly used POPE [?] benchmark.

**Baselines.** We compare ForensicZip against state-of-the-art training-free token pruning methods and full-token expert models: **1) Training-free Token Pruning Methods:** We benchmark against leading inference acceleration strategies, including FastV [4], SparseVLM [46], and recent SOTAs such as VisionTrim [42] and LLaVA-Scissor [31]. **2) Forensic Expert Models (Vanilla):** We report the upper-bound performance using the full-token versions of state-of-the-art

**Table 2: Efficiency comparisons on the FakeClue dataset.** LLM Generation Latency: time for LLM-only response generation; Model Generation Latency: time for the full model to generate response; Total Latency: total time to complete the FakeClue benchmark; GPU Peak Memory: maximum VRAM usage during inference; and Throughput: number of samples processed per second. Comparisons are conducted at **25% token retention**.

Methods	LLM Generation↓	Model Generation↓	Total↓	GPU Peak↓	Throughput↑	Performance↑
	Latency (s)	Latency (s)	Latency (min:sec)	Memory (GB)	(samples/s)	Acc (%)
<i>FakeVLM-7B (Vanilla)</i>	1472.5	1478.6	67:59	26.7	1.23	98.60
<b>Retention Ratio = 25%</b>						
<b>FastV</b> [ECCV'24]	885.2 (↓ 39.9%)	892.4 (↓ 39.6%)	41:30 (↓ 38.9%)	26.5 (↓ 0.7%)	2.00 (↑ 1.63×)	82.34 (↓ 16.2)
<b>SparseVLM</b> [ICML'25]	870.5 (↓ 40.9%)	878.2 (↓ 40.6%)	40:55 (↓ 39.8%)	26.6 (↓ 0.4%)	2.03 (↑ 1.65×)	85.63 (↓ 12.9)
<b>LLaVA-Scissor</b> [NeurIPS'25]	852.1 (↓ 42.1%)	860.5 (↓ 41.8%)	40:10 (↓ 40.9%)	26.5 (↓ 0.7%)	2.07 (↑ 1.68×)	91.45 (↓ 7.1)
<b>VisionTrim</b> [ICLR'26]	835.4 (↓ 43.3%)	842.1 (↓ 43.0%)	39:45 (↓ 41.5%)	26.4 (↓ 1.1%)	2.10 (↑ 1.71×)	94.83 (↓ 3.7)
<b>ForensicZip (Ours)</b>	<b>660.5</b> (↓ 55.1%)	<b>666.8</b> (↓ 54.9%)	<b>30:55</b> (↓ 54.5%)	<b>19.8</b> (↓ 25.8%)	<b>2.70</b> (↑ 2.20×)	<b>98.46</b> (↓ 0.1)

**Table 3: Comprehensive efficiency and performance results on the POPE [?] benchmark.** Comparison of generation latency, end-to-end time, peak GPU memory, throughput, and accuracy on a single NVIDIA A100 GPU.

Backbone	Method	#Tokens	LLM Gen.	Total Lat.	Peak Mem.	Throughput	FLOPs	Acc. ↑
			Lat. (s) ↓	(min:sec) ↓	(GB) ↓	(samples/s) ↑	(T) ↓	
<b>LLaVA-1.5-7B</b>	Vanilla	576	618.0	21:43 (1.00×)	18.5	0.64	3.8	85.9
	+ SparseVLM (ICML'25)	64	512.4	18:24 (1.18×)	20.2	0.76	1.3	75.1
	+ VisionTrim (ICLR'26)	64	448.5	16:10 (1.34×)	19.1	0.86	1.0	84.5
	+ <b>ForensicZip (Ours)</b>	<b>64</b>	<b>412.0</b>	<b>14:52 (1.46×)</b>	<b>16.8</b>	<b>0.94</b>	<b>0.8</b>	<b>86.1</b>
<b>LLaVA-NeXT-7B</b>	Vanilla	2880	1008.4	38:04 (1.00×)	46.2	0.35	12.6	86.3
	+ SparseVLM (ICML'25)	320	846.2	31:43 (1.20×)	48.5	0.42	2.5	78.5
	+ VisionTrim (ICLR'26)	320	625.4	21:50 (1.74×)	42.0	0.61	1.8	83.5
	+ <b>ForensicZip (Ours)</b>	<b>320</b>	<b>520.8</b>	<b>18:28 (2.06×)</b>	<b>36.5</b>	<b>0.72</b>	<b>1.2</b>	<b>85.8</b>

forensic MLLMs, SIDA [18], FakeVLM [36] and FakeShield [40] to demonstrate that ForensicZip retains expert-level capability under extreme compression.

**Implementation Details.** We adopt LLaVA-OneVision-7B [21], SIDA-7B/13B [18], FakeVLM [36] and FakeShield [40] as our primary backbones. The Transport Novelty Estimation (TNE) utilizes entropic regularization  $\varepsilon = 0.1$ , with birth and death costs set to  $c_{\text{birth}} = c_{\text{death}} = 0.35$ . All experiments are conducted on NVIDIA A100 (80GB) GPUs.

**Performance on Forensic Benchmarks.** We evaluate ForensicZip against leading training-free pruning baselines across diverse forgery types. As summarized in Tables 1 and ??, existing semantic-driven methods (FastV, SparseVLM) maintain competitive accuracy at conservative retention ratios but suffer catastrophic performance collapse as the token budget decreases. Specifically, at an aggressive 10% retention ratio, these baselines degrade to near-random performance on the FakeClue and SID-Set benchmarks. In contrast, ForensicZip establishes a superior efficiency-accuracy frontier, maintaining 97.74% accuracy on FakeClue with only 10% visual tokens and scaling effectively to larger SIDA-13B backbones. This stability corroborates our core hypothesis: forensic evidence typically resides in semantically sparse regions. By prioritizing physical inconsistency rather than conceptual saliency, our transport-based scoring successfully preserves critical manipulation traces that are systematically filtered out by attention-based metrics.

**Efficiency and Robustness Analysis.** We assess efficiency through both deployment latency and downstream reasoning stability. Unlike masking-based techniques that reduce attention complexity but retain full sequence lengths in FFN layers, ForensicZip implements physical token elimination. Table 2 confirms this design advantage: peak GPU memory consumption drops from 26.7GB to 19.8GB on LLaVA-OV-7B, translating to a 2.20× throughput improvement. Furthermore, evaluation on the POPE object hallucination benchmark (Table 3) reveals an unexpected benefit: ForensicZip slightly improves the accuracy of the vanilla LLaVA-1.5 model (86.1 vs 85.9). We attribute this precision gain to the removal of redundant semantic noise, which prevents the MLLM from over-focusing on irrelevant background context, thereby providing a cleaner evidence set for reasoning.

**Ablation Study.** We validate component efficacy on the SID-Set benchmark (Table 4). Base semantic pruning yields poor results (57.20% accuracy); introducing Transport Novelty Estimation (TNE) captures temporal dynamics, significantly boosting performance to 83.40%. Table 5 further investigates the transport formulation: standard balanced OT smears forensic signals by forcing spurious correspondences, whereas our augmented Birth-Death mechanism explicitly isolates unmatched artifacts via dummy nodes, yielding a substantial +16.31% relative gain. Finally, Table 6 indicates that the isotropic Laplacian operator outperforms directional filters, suggesting that generative artifacts manifest as non-directional high-frequency anomalies best captured by rotation-invariant second-order derivatives.

**Table 4: Ablation study of core components in ForensicZip.** Evaluated on the **SID-Set** benchmark using the **SIDA-7B** backbone at a **10% token retention** ratio. We incrementally validate the effectiveness of Transport Novelty Estimation (TNE) and Forensic Scoring (FS). **Base** uses FastV semantic attention ranking with physical Top- $K$  pruning (global token always kept) under the same token budget.

Variant	Components			Real Images		Tampered Images		Overall Performance	
	TNE	FS	HF	Acc	F1	Acc	F1	Acc	F1
(a) Base				55.23	52.45	54.23	51.56	57.20	54.95
(b) + TNE	✓			80.10	78.60	82.20	80.30	83.40	82.10
(c) + FS	✓	✓		85.60	87.40	88.20	87.90	90.10	89.90
<b>(d) ForensicZip</b>	✓	✓	✓	<b>88.15</b>	<b>90.10</b>	<b>90.35</b>	<b>90.15</b>	<b>92.50</b>	<b>92.52</b>

**Table 5: Effect of Transport Formulations in TNE.** Evaluated on **SID-Set** with **SIDA-7B** (10% retention). Explicitly modeling unmatchable tokens via dummy nodes is crucial for capturing generative artifacts.

Alignment Strategy	Synthetic		Overall		Rel. Gain
	Acc	F1	Acc	F1	
Hard Assignment	86.40	86.00	79.54	79.10	—
Balanced OT	92.90	92.70	86.10	85.80	+8.25%
Only-Birth Penalty	95.80	95.60	89.20	88.90	+12.15%
<b>Birth-Death OT</b>	<b>97.95</b>	<b>97.85</b>	<b>92.50</b>	<b>92.52</b>	<b>+16.31%</b>

**Table 6: Effect of Spatial Operators in FS.** Evaluated on **FakeClue** using **FakeVLM-7B** (10% retention). Laplacian ( $\mathcal{L}$ ) yields the best preservation of localized noise by providing isotropic high-frequency priors.

Spatial Operator $\mathcal{L}(\cdot)$	Accuracy (%)	Rel. Gain
None ( $\eta_{\text{forensic}} = 0$ )	93.45	—
Patch Variance (RGB)	94.82	+1.47%
Sobel (Directional)	96.15	+2.89%
<b>Laplacian (Isotropic, Ours)</b>	<b>97.74</b>	<b>+4.59%</b>

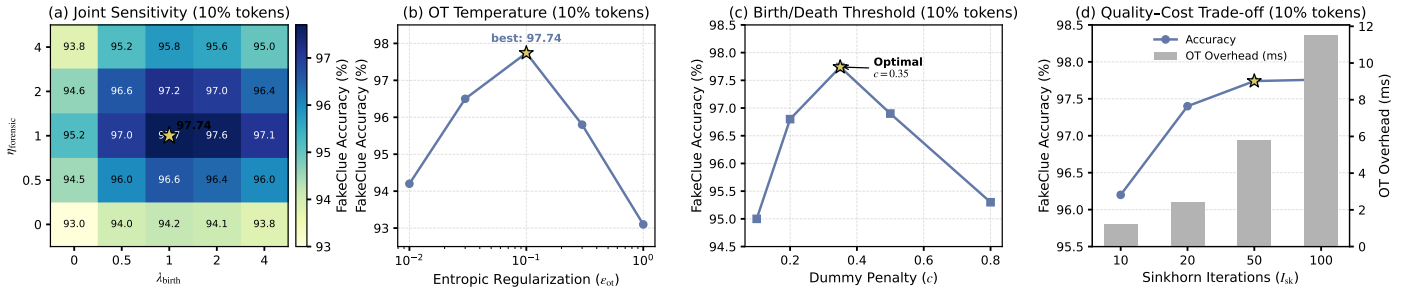


**Fig. 4: Ablation Study.** Impact of (a) joint weights  $\lambda/\eta$ , (b) regularization  $\epsilon_{\text{ot}}$ , (c) penalty  $c$ , and (d) iterations on FakeClue accuracy.

**Hyperparameter Sensitivity.** Fig. 4 analyzes the impact of joint weights ( $\lambda/\eta$ ), transport penalty ( $c$ ), regularization ( $\epsilon$ ), and solver iterations. The performance remains stable across broad ranges (a-c), confirming the robustness of our dual-domain scoring.

## 5 Conclusion

In this paper, we propose ForensicZip, a training-free and forgery-aware inference acceleration framework for forensic Vision-Language Models. Our insight for ForensicZip arises from our observation that forensic evidence is often spatially orthogonal to semantic saliency and manifests as temporal discontinuities in the token space. ForensicZip formulates temporal token evolution as an augmented birth death optimal transport problem to explicitly quantify transient artifacts, which results in significant computational cost reduction while preserving critical forensic cues even under aggressive compression.

## References

- Alvar, S.R., Singh, G., Akbari, M., Zhang, Y.: Divprune: Diversity-based visual token pruning for large multimodal models. In: Proceedings of the Computer Vision and Pattern Recognition Conference. pp. 9392–9401 (2025) **1, 2, 3**
- Bai, J., Bai, S., Yang, S., Wang, S., Tan, S., Wang, P., Lin, J., Zhou, C., Zhou, J.: Qwen-vl: A frontier large vision-language model with versatile abilities. arXiv preprint arXiv:2308.12966 (2023) **1**
- Bolya, D., Fu, C.Y., Dai, X., Zhang, P., Feichtenhofer, C., Hoffman, J.: Token merging: Your vit but faster. arXiv preprint arXiv:2210.09461 (2022) **3**

4. Chen, L., Zhao, H., Liu, T., Bai, S., Lin, J., Zhou, C., Chang, B.: An image is worth 1/2 tokens after layer 2: Plug-and-play inference acceleration for large vision-language models. In: European Conference on Computer Vision. pp. 19–35. Springer (2024) [1](#), [2](#), [6](#)
5. Chen, L., Zhao, H., Liu, T., Bai, S., Lin, J., Zhou, C., Chang, B.: An image is worth 1/2 tokens after layer 2: Plug-and-play inference acceleration for large vision-language models. In: ECCV. pp. 19–35. Springer (2024) [2](#)
6. Chen, Y., Yan, Z., Cheng, G., Zhao, K., Lyu, S., Wu, B.: X2-dfd: A framework for explainable and extendable deepfake detection. arXiv preprint arXiv:2410.06126 (2024) [1](#), [2](#)
7. Chollet, F.: Xception: Deep learning with depthwise separable convolutions. In: CVPR (2017) [2](#)
8. Chu, X., Qiao, L., Lin, X., Xu, S., Yang, Y., Hu, Y., Wei, F., Zhang, X., Zhang, B., Wei, X., et al.: Mobilevlm: A fast, reproducible and strong vision language assistant for mobile devices. arXiv:2312.16886 (2023) [1](#)
9. Corvi, R., Cozzolino, D., Zingarini, G., Poggi, G., Nagano, K., Verdoliva, L.: On the detection of synthetic images generated by diffusion models. In: ICASSP 2023-2023 IEEE International Conference on Acoustics, Speech and Signal Processing (ICASSP). pp. 1–5. IEEE (2023) [6](#)
10. Dang, H., Liu, F., Stehouwer, J., Liu, X., Jain, A.K.: On the detection of digital face manipulation. In: Proceedings of the IEEE/CVF Conference on Computer Vision and Pattern Recognition. pp. 5781–5790 (2020) [6](#)
11. Dong, J., Wang, W., Tan, T.: Casia image tampering detection evaluation database. In: Proceedings of the IEEE China Summit and International Conference on Signal and Information Processing (ChinaSIP) (2013) [6](#)
12. Fu, C., Chen, P., Shen, Y., Qin, Y., Zhang, M., Lin, X., Qiu, Z., Lin, W., Yang, J., Zheng, X., Li, K., Sun, X., Ji, R.: Mme: A comprehensive evaluation benchmark for multimodal large language models. arXiv preprint arXiv:2306.13394 (2023) [1](#)
13. Fu, X., Yan, Z., Yao, T., Chen, S., Li, X.: Exploring unbiased deepfake detection via token-level shuffling and mixing. In: AAAI (2025) [3](#)
14. Guo, X., Liu, X., Masi, I., Liu, X.: Language-guided hierarchical fine-grained image forgery detection and localization. International Journal of Computer Vision **133**(5), 2670–2691 (2025) [2](#)
15. Guo, X., Song, X., Zhang, Y., Liu, X., Liu, X.: Rethinking vision-language model in face forensics: Multi-modal interpretable forged face detector. In: Proceedings of the Computer Vision and Pattern Recognition Conference. pp. 105–116 (2025) [1](#), [2](#)
16. Han, Y., Liu, X., Zhang, Z., Ding, P., Chen, J., Wang, D., Chen, H., Yan, Q., Huang, S.: Filter, correlate, compress: Training-free token reduction for mllm acceleration. arXiv preprint arXiv:2411.17686 (2024) [1](#), [2](#)
17. Heo, Y.J., Choi, Y.J., Lee, Y.W., Kim, B.G.: Deepfake detection scheme based on vision transformer and distillation. arXiv preprint arXiv:2104.01353 (2021) [2](#)
18. Huang, Z., Hu, J., Li, X., He, Y., Zhao, X., Peng, B., Wu, B., Huang, X., Cheng, G.: Sida: Social media image deepfake detection, localization and explanation with large multimodal model. arXiv preprint arXiv:2412.04292 (2024) [6](#), [7](#)
19. Huang, Z., Hu, J., Li, X., He, Y., Zhao, X., Peng, B., Wu, B., Huang, X., Cheng, G.: Sida: Social media image deepfake detection, localization and explanation with large multimodal model. In: Proceedings of the Computer Vision and Pattern Recognition Conference. pp. 28831–28841 (2025) [1](#), [2](#)
20. Kang, H., Wen, S., Wen, Z., Ye, J., Li, W., Feng, P., Zhou, B., Wang, B., Lin, D., Zhang, L., et al.: Legion: Learning to ground and explain for synthetic image detection. In: Proceedings of the IEEE/CVF International Conference on Computer Vision. pp. 18937–18947 (2025) [2](#)
21. Li, B., Zhang, Y., Guo, D., Zhang, R., Li, F., Zhang, H., Zhang, K., Zhang, P., Li, Y., Liu, Z., et al.: Llava-onevision: Easy visual task transfer. arXiv preprint arXiv:2408.03326 (2024) [7](#)
22. Li, K., Chen, X., Gao, C., Li, Y., Chen, X.: Balanced token pruning: Accelerating vision language models beyond local optimization. arXiv preprint arXiv:2505.22038 (2025) [1](#), [2](#)
23. Lin, B., Ye, Y., Zhu, B., Cui, J., Ning, M., Jin, P., Yuan, L.: Video-llava: Learning united visual representation by alignment before projection. arXiv preprint arXiv:2311.10122 (2023) [1](#)
24. Liu, H., Li, C., Li, Y., Lee, Y.J.: Improved baselines with visual instruction tuning. In: CVPR. pp. 26296–26306 (2024) [1](#)
25. Liu, H., Li, C., Li, Y., Li, B., Zhang, Y., Shen, S., Lee, Y.J.: Llava-next: Improved reasoning, ocr, and world knowledge (2024), <https://llava-vl.github.io/blog/2024-01-30-llava-next/> [1](#)
26. Liu, X., Wang, Z., Chen, J., Han, Y., Wang, Y., Yuan, J., Song, J., Huang, S., Chen, H.: Global compression commander: Plug-and-play inference acceleration for high-resolution large vision-language models. arXiv preprint arXiv:2501.05179 (2025) [2](#)
27. Shang, Y., Cai, M., Xu, B., Lee, Y.J., Yan, Y.: Llava-prumerge: Adaptive token reduction for efficient large multimodal models. arXiv preprint arXiv:2403.15388 (2024) [1](#)
28. Shang, Y., Cai, M., Xu, B., Lee, Y.J., Yan, Y.: Llava-prumerge: Adaptive token reduction for efficient large multimodal models. In: Proceedings of the IEEE/CVF International Conference on Computer Vision. pp. 22857–22867 (2025) [1](#)
29. Shao, R., Wu, T., Liu, Z.: Detecting and recovering sequential deepfake manipulation. In: European Conference on Computer Vision. pp. 712–728. Springer (2022) [2](#)
30. Song, X., Guo, X., Zhang, J., Li, Q., Bai, L., Liu, X., Zhai, G., Liu, X.: On learning multi-modal forgery representation for diffusion generated video detection. Advances in Neural Information Processing Systems **37**, 122054–122077 (2024) [2](#)
31. Sun, B., Zhao, J., Wei, X., Hou, Q.: Llava-scissor: Token compression with semantic connected components for video llms. arXiv preprint arXiv:2506.21862 (2025) [1](#), [2](#), [6](#)
32. Tan, H., Lan, J., Tan, Z., Liu, A., Song, C., Shi, S., Zhu, H., Wang, W., Wan, J., Lei, Z.: Veritas: Generalizable deepfake detection via pattern-aware reasoning. arXiv preprint arXiv:2508.21048 (2025) [1](#), [2](#)
33. Wang, P., Bai, S., Tan, S., Wang, S., Fan, Z., Bai, J., Chen, K., Liu, X., Wang, J., Ge, W., Fan, Y., Dang, K., Du, M., Ren, X., Men, R., Liu, D., Zhou, C., Zhou, J., Lin, J.: Qwen2-vl: Enhancing vision-language model’s perception of the world at any resolution. arXiv preprint arXiv:2409.12191 (2024) [1](#)

34. Wang, S.Y., Wang, O., Owens, A., Zhang, R., Efros, A.A.: Detecting photoshopped faces by scripting photoshop. In: ICCV (2019) [2](#)
35. Wang, S.Y., Wang, O., Zhang, R., Owens, A., Efros, A.A.: Cnn-generated images are surprisingly easy to spot...for now. In: CVPR (2020) [2](#)
36. Wen, S., Ye, J., Feng, P., Kang, H., Wen, Z., Chen, Y., Wu, J., Wu, W., He, C., Li, W.: Spot the fake: Large multimodal model-based synthetic image detection with artifact explanation. arXiv preprint arXiv:2503.14905 (2025) [1](#), [2](#), [7](#)
37. Wen, Z., Gao, Y., Li, W., He, C., Zhang, L.: Token pruning in multimodal large language models: Are we solving the right problem? arXiv preprint arXiv:2502.11501 (2025) [1](#), [2](#), [3](#)
38. Wen, Z., Wang, S., Zhou, Y., Zhang, J., Zhang, Q., Gao, Y., Chen, Z., Wang, B., Li, W., He, C., et al.: Efficient multi-modal large language models via progressive consistency distillation. arXiv preprint arXiv:2510.00515 (2025) [1](#)
39. Xu, R., Wang, Y., Luo, Y., Du, B.: Rethinking visual token reduction in lvlms under cross-modal misalignment. arXiv preprint arXiv:2506.22283 (2025) [1](#)
40. Xu, Z., Zhang, X., Li, R., Tang, Z., Huang, Q., Zhang, J.: Fakeshield: Explainable image forgery detection and localization via multi-modal large language models. arXiv preprint arXiv:2410.02761 (2024) [1](#), [2](#), [6](#), [7](#)
41. Ye, J., Zhou, B., Huang, Z., Zhang, J., Bai, T., Kang, H., He, J., Lin, H., Wang, Z., Wu, T., et al.: Loki: A comprehensive synthetic data detection benchmark using large multimodal models. In: ICLR (2025) [6](#)
42. Yu, H., Li, W., Qu, X., Wang, S., Chen, J., Zhu, J.: Visiontrim: Unified vision token compression for training-free mllm acceleration. arXiv preprint arXiv:2601.22674 (2026) [1](#), [3](#), [6](#)
43. Yu, Z., Xu, D., Yu, J., Yu, T., Zhao, Z., Zhuang, Y., Tao, D.: Activitynet-qa: A dataset for understanding complex web videos via question answering. In: AAAI. vol. 33, pp. 9127–9134 (2019) [1](#)
44. Yue, X., Ni, Y., Zhang, K., Zheng, T., Liu, R., Zhang, G., Stevens, S., Jiang, D., Ren, W., Sun, Y., et al.: Mmmu: A massive multi-discipline multimodal understanding and reasoning benchmark for expert agi. In: Proceedings of the IEEE/CVF Conference on Computer Vision and Pattern Recognition. pp. 9556–9567 (2024) [1](#)
45. Zhang, Q., Liu, M., Li, L., Lu, M., Zhang, Y., Pan, J., She, Q., Zhang, S.: Beyond attention or similarity: Maximizing conditional diversity for token pruning in mllms. arXiv preprint arXiv:2506.10967 (2025) [1](#), [3](#)
46. Zhang, Y., Fan, C.K., Ma, J., Zheng, W., Huang, T., Cheng, K., Gudovskiy, D., Okuno, T., Nakata, Y., Keutzer, K., et al.: Sparsevlm: Visual token sparsification for efficient vision-language model inference. In: ICML. PMLR (2025) [1](#), [2](#), [6](#)
47. Zhang, Y., Colman, B., Guo, X., Shahriyari, A., Bharaj, G.: Common sense reasoning for deepfake detection. In: European Conference on Computer Vision. pp. 399–415. Springer (2024) [2](#), [6](#)
48. Zhong, Y., Liu, Z., Li, Y., Wang, L.: Aim: Adaptive inference of multi-modal llms via token merging and pruning. arXiv preprint arXiv:2412.03248 (2024) [1](#), [2](#)
49. Zhou, B., Yang, H., Chen, D., Ye, J., Bai, T., Yu, J., Zhang, S., Lin, D., He, C., Li, W.: Urbench: A comprehensive benchmark for evaluating large multimodal models in multi-view urban scenarios. In: Proceedings of the AAAI Conference on Artificial Intelligence. vol. 39, pp. 10707–10715 (2025) [1](#)
50. Zhou, Z., Luo, Y., Wu, Y., Sun, K., Ji, J., Yan, K., Ding, S., Sun, X., Wu, Y., Ji, R.: Aigi-holmes: Towards explainable and generalizable ai-generated image detection via multimodal large language models. In: Proceedings of the IEEE/CVF International Conference on Computer Vision. pp. 18746–18758 (2025) [1](#), [2](#)